Bioorganic & Medicinal Chemistry 17 (2009) 811–819

Contents lists available at ScienceDirect

Bioorganic & Medicinal Chemistry

journal homepage: www.elsevier.com/locate/bmc

# The stereochemistry of *N*-methyl and aryl substituents determine the biological activities of 3-aryl-8-methyl-8-azabicyclo[3.2.1]oct-2,3-enes

Aleksej Krunić [a], Dahua Pan [a], William J. Dunn III [a], S. V. Santhana Mariappan [b,*]

[a] Department of Medicinal Chemistry & Pharmacognosy, College of Pharmacy MC 781, University of Illinois at Chicago, 833 S. Wood St. Rm 539, Chicago, IL 60612-7231, USA
[b] Department of Chemistry, College of Liberal Arts and Sciences, CB-181, University of Iowa, Iowa City, IA 52242-1294, USA

ARTICLE INFO

*Article history:*
Received 25 August 2008
Revised 12 November 2008
Accepted 14 November 2008
Available online 20 November 2008

*Keywords:*
Monoamine transporters
Dopamine
Serotonin
Epinephrine
Aryl tropanes
Nitrogen inversion
Ligand conformation
Nuclear magnetic resonance
Nuclear Overhauser effect
Molecular modeling

ABSTRACT

Aryl substituted tropanes and their 2,3-ene analogs are highly selective inhibitors of monoamine uptake. The solution structures of a series of aryl tropanes were determined using NMR spectroscopy and molecular modeling to identify conformational preferences that may determine the overall activity. The majority of these analogs undergo nitrogen inversion, and the rate of interconversion between the *axial* and *equatorial* *N*-methyl conformers is fast on the NMR timescale at room temperature but slow between 217 and 243 K allowing us to determine the thermodynamic parameters of interconversion using dynamic and magnetization transfer NMR. The biological activities correlate strongly with the nature and the orientation of the aryl group. The relative orientation of the *N*-methyl further modulates the activity by directly influencing the ligand interaction in the protein binding pocket and/or by forcing a favorable orientation for the aryl substituent to fit in the binding pocket.

Published by Elsevier Ltd.

## 1. Introduction

Monoamine transporters (MAT) play a crucial role in the formation of cocaine abuse and other neurological disorders rendering them as targets for therapeutic intervention.[1–3] Three-dimensional structures of monoamine transporters are currently unknown. Among the various classes of potential pharmacological agents phenyl tropanes (Fig. 1) are probably the largest and most studied series of cocaine analogs. Pharmacologically, phenyltropanes are similar to cocaine (Fig. 1),[4] and are commonly used as radioligands in binding studies. The SAR data on this class of compounds are extensive and the subject of numerous reviews.[5]

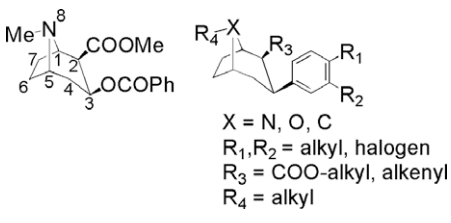


**Figure 1.** Structure of (*R*)-cocaine and the phenyl tropane analogs.

The unsubstituted phenyl tropane ($R_1 = R_2 = H$, $R_3 = COOMe$, $R_4 = Me$,) was 4.4 times more potent than cocaine which was attributed to the reduced interatomic distance between the nitrogen N8 and the centroid of the aromatic ring as compared to cocaine.[6,7] Substituents on the aromatic ring modify the selectivity for individual transporters, dopamine (DAT) or serotonin (SERT); the isopropyl analog displayed 5-fold selectivity for the SERT over the DAT.[6,7] The 3′,4′-disubstituted phenyl tropanes contained some of the most potent analogs ($R_1 = Cl$, Me, $R_2 = Cl$).[7–9] The role of a phenyl group was further probed by extending to compounds containing two aromatic rings linked by a variable number of carbon atoms (Fig. 2).[10] Compounds consisting of a two carbon linker were the most potent (3–5 nM) and selective for DAT. Increasing the

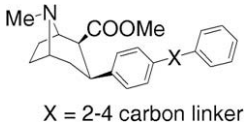


**Figure 2.** General formula for 4′-substituted 3β-phenyltropane analogs. Two phenyl rings are connected via an aliphatic spacer with variable lengths.

* Corresponding author. Tel.: +1 319 335 1336, fax: +1 319 335 2291.
*E-mail address:* santhana-velupillai@uiowa.edu (S.V. Santhana Mariappan).

0968-0896/$ - see front matter Published by Elsevier Ltd.
doi:10.1016/j.bmc.2008.11.038

number of carbons led to a loss of activity. These results suggest that a remote binding site exists in the DAT binding domains, which extends out approximately two carbons from the tropane 3β-phenyl ring. This space is limited and apparently ends abruptly as evidenced by the significant loss of binding affinity in those compounds which possess one and two additional methylene groups.

A recent molecular field analysis (MFA) examined the effect of ligand conformation, and the results again support the role of the aryl group in determining the biological activity of monoamine transporters.[11] The conformational preferences of the ligands may also further modulate the biological activities, as recently reported for morphine alkaloids by Belostotskii et al.[12]

The orientation of the electron lone pair of N8 also plays a crucial role in determining the bioactivity of the aryl tropanes. Smith et al. demonstrated recently that axial and *equatorial* orientations of the lone pair, relative to the piperidine ring, offered high affinity and selectivity toward DAT and SERT, respectively, using rigid tricyclic phenyl tropane analogs.[13] However, in flexible and semi-rigid aryl tropanes, the orientation of the electron lone pair is not known, and must be determined in order to make reliable correlations. The orientation of the *N*-methyl determines the positioning of electron lone pair and vice versa; therefore, characterization of the *N*-methyl orientation will reveal the orientation of the electron lone pair by default. The orientation of the *N*-methyl group in aryl tropanes has been studied by X-ray crystallography, NMR, and theoretical studies.[14–18] Whereas the X-ray crystallographic and computational studies support a preference for the *equatorial* orientation, NMR studies on a number of tropane analogs reveal the presence of both *equatorial* and *axial* forms; the relative population and the equilibrium constants for the interconversion depend on the nature of the ligand, temperature, and solution conditions.[19–22]

Recently, we reported the syntheses and biological activities of a number of semi-rigid 3-aryl-8-methyl-8-azabicyclo[3.2.1]oct-2-enes (3-aryltropanes) without the 2-subsitutents.[23] The ligands with 2,3-double bond were active and selective toward human SERT (hSERT) over human DAT (hDAT) and human NET (hNET), respectively. These ligands were designed with the aim to determine the nature of the aromatic binding pocket of the transporter proteins and to determine the correlation between the orientation of the *N*-methyl group and the biological activity. Herein, we report their solution conformations, the thermodynamics of nitrogen inversion (*equatorial*-to-*axial* *N*-methyl) and the correlation of structural and thermodynamic parameters with the bioactivity. The activation energy barrier or other thermodynamic parameters for the nitrogen inversion in the 2,3-unsaturated 3-aryltropane series have not been determined experimentally and the effect of 3-aryl substituent on the *N*-methyl equilibrium is mostly unknown. Furthermore, the measurement of thermodynamic parameters of nitrogen inversion for similar compounds may lead to new thermodynamics-activity relationships or spectroscopy-derived activity relationships.

## 2. Results and discussion

Figure 3 shows the structures of 3-aryltropanes that were investigated in this study. These compounds are broadly divided into two categories distinguished by the presence of either C2–C3 double bond or the C3–OH. Tables 1 and 2 list the $^{1}H$ and $^{13}C$ chemical shifts, whereas Figure 4 shows a representative NOE cross-section for **8**. The NOEs observed between the aromatic (H1′ and H3′) and the tropane H2 proton (Fig. 4) demonstrate that they are close in space and are sensitive to changes in the relative orientation of the aryl group with respect to the tropane skeleton.

### 2.1. Dynamic NMR

In order to determine whether multiple conformations are present due to nitrogen inversion (Fig. 5) and/or due to restricted rotation of the C–C single bond connecting the tropane and the aryl group, $^{1}H$ and $^{13}C$ NMR spectra were collected over a temperature range of 217–300 K. Alkene derivatives were found to show resonance doubling at low temperatures both in $^{1}H$ and $^{13}C$ spectra. The resonance doubling was absent for 3-OH derivatives in the entire temperature range indicating either there was no conformational mixture or the rate of interconversion was faster than the NMR time scale.

Only a single set of NMR signals was detected for the semi-rigid 3-aryl tropanes **1**, **4**, **6**, **8**, **9**, and **10** at room temperature due to a fast interconversion between the two orientations of the *N*-methyl group. However, at temperatures below 243 K, $^{1}H$ resonance doubling occurred for the methyl, alkene and $H4_{ax}$ protons as a result of two coexisting structural forms. Figure 6 shows temperature-dependent $^{1}H$ NMR spectra and their respective NOE cross-sections for **8**. The exchange rate between conformations is slow on the NMR time scale under these conditions.

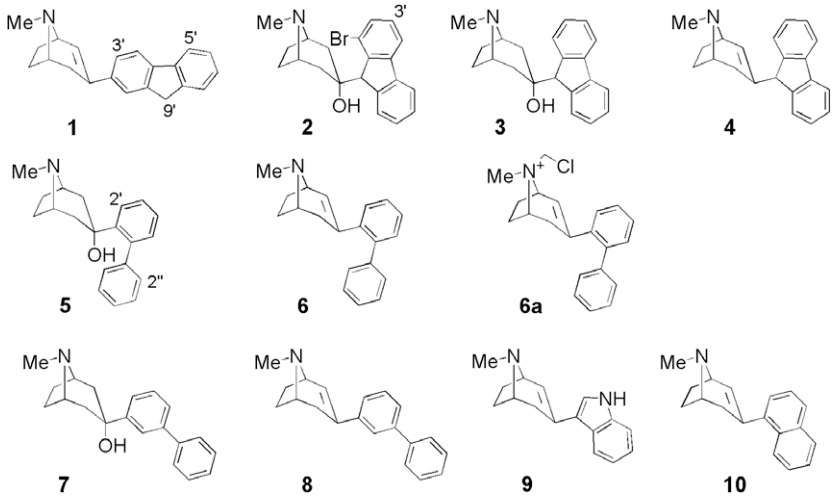


**Figure 3.** Structures and the numbering scheme of the 3-aryl-substituted 8-methyl-8-azabicyclo[3.2.1]octanes (3-aryltropanes) used in this study.

**Table 1**
Proton chemical shifts (ppm) for compounds **1–9**

| Proton | Compound | | | | | | | | | |
|---|---|---|---|---|---|---|---|---|---|---|
| | **1** | **2** | **3** | **4** | **5** | **6** | **6a** | **7** | **8** | **9** |
| H1 | 3.47 | 3.20 | 3.14 | 3.40 | 3.14 | 3.42 | 4.72 | 3.27 | 3.43 | 3.51 |
| H2 | 6.33 | 1.46, 2.21 | 1.25, 2.11 | 6.12 | 1.80, 2.47 | 5.77 | 5.88 | 1.85, 2.49 | 6.43 | 6.37 |
| H4 | 2.09, 2.96 | 1.02, 2.02 | 1.25, 2.11 | 0.76, 1.86 | 1.80, 2.47 | 1.49, 2.42 | 2.13, 2.79 | 1.85, 2.49 | 2.11, 2.96 | 2.03, 2.90 |
| H5 | 3.47 | 3.12 | 3.14 | 3.02 | 3.14 | 3.21 | 5.00 | 3.27 | 3.43 | 3.40 |
| H6 | 1.95, 2.15 | 1.28, 2.02 | 1.88, 1.95 | 1.96, 2.05 | 1.86, 2.02 | 1.86, 2.05 | 2.25, 2.40 | 2.05, 2.25 | 1.72, 2.12 | 1.68, 2.17 |
| H7 | 1.65, 2.15 | 1.20, 2.02 | 1.88, 1.95 | 1.35, 2.05 | 1.86, 2.02 | 1.28, 2.05 | 1.74, 2.44 | 2.05, 2.25 | 1.64, 2.22 | 1.97, 2.17 |
| *N*-Me | 2.45 | 2.12 | 2.08 | 2.40 | 2.29 | 2.42 | 3.46 | 2.36 | 2.43 | 2.48 |
| H1′ | 7.58 | 7.94 | — | 7.48 | — | — | — | — | — | — |
| H2′ | — | — | 7.34 | 7.30 | — | — | — | 7.76 | — | 7.12 |
| H3′ | 7.42 | 7.47 | 7.25 | 7.39 | 7.52 | 7.24 | 7.18 | — | 7.58 | — |
| H4′ | 7.72–7.76 | 7.56 | 7.69 | 7.76 | 7.30 | 7.30 | 7.41–7.45 | 7.53 | 7.37 | 7.92 |
| H5′ | | 7.67 | 7.69 | 7.76 | 7.18 | 7.36 | | 7.37 | 7.34 | 7.15 |
| H6′ | 7.37 | 7.32 | 7.34 | 7.30 | 7.02 | 7.30 | 7.35 | 7.44 | 7.37 | 7.18 |
| H7′ | 7.29 | 7.26 | 7.25 | 7.39 | — | — | — | — | — | 7.37 |
| H8′ | 7.54 | 7.67 | 7.74 | 7.48 | — | — | — | — | — | — |
| H9′ | 3.89 | 3.97 | 4.00 | 4.45 | — | — | — | — | — | — |
| H2″ | — | — | — | — | 7.37 | 7.36 | 7.28 | 7.60 | 7.58 | — |
| H3″ | — | — | — | — | 7.37 | 7.36 | 7.41–7.45 | 7.41 | 7.43–7.44 | — |
| H4″ | — | — | — | — | 7.30 | 7.30 | | 7.33 | | — |
| H5″ | — | — | — | — | 7.37 | 7.36 | | 7.41 | | — |
| H6″ | — | — | — | — | 7.37 | 7.36 | 7.28 | 7.60 | 7.58 | — |
| H9 | — | — | — | — | — | — | 5.46–6.02 | — | — | — |
| N1′ | — | — | — | — | — | — | — | — | — | 8.38 |

**Table 2**
$^{13}$C chemical shifts (ppm) for compounds **1–9**

| Proton | Compound | | | | | | | | | |
|---|---|---|---|---|---|---|---|---|---|---|
| | **1** | **2** | **3** | **4** | **5** | **6** | **6a** | **7** | **8** | **9** |
| 1 | 59.87 | 59.07 | 59.16 | 59.19 | 60.88 | 59.24 | 66.47 | 61.01 | 59.36 | 59.30 |
| 2 | 126.51 | 42.65 | 42.65 | 128.62 | 46.13 | 129.32 | 124.45 | 45.55 | 127.42 | 125.12 |
| 3 | 140.85 | 73.03 | 73.18 | 73.17 | 75.13 | 136.57 | 145.15 | 72.97 | 132.40 | 127.45 |
| 4 | 34.11 | 42.15 | 42.65 | 28.85 | 46.13 | 34.80 | 37.57 | 45.55 | 33.07 | 34.24 |
| 5 | 58.25 | 58.94 | 59.16 | 56.90 | 60.88 | 57.89 | 67.30 | 61.01 | 57.53 | 57.96 |
| 6 | 33.80 | 29.64 | 29.19 | 34.70 | 25.38 | 33.57 | 32.39 | 25.54 | 33.67 | 33.75 |
| 7 | 30.23 | 29.18 | 29.19 | 29.70 | 25.38 | 29.09 | 27.90 | 25.54 | 29.83 | 29.75 |
| *N*-Me | 36.50 | 40.53 | 40.43 | 35.75 | 40.23 | 35.58 | 40.67 | 40.39 | 36.47 | 36.70 |
| 1′ | 121.26 | 130.79 | 127.69 | 124.49 | 140.20 | 140.23 | 140.70 | 141.61 | 141.33 | |
| 2′ | 132.66 | 120.92 | 127.56 | 127.29 | 146.55 | 140.62 | 139.49 | 123.49 | 123.77 | 121.48 |
| 3′ | 123.52 | 130.28 | 126.99 | 127.31 | 126.40 | 129.01 | 128.73 | 150.64 | 132.40 | 117.41 |
| 4′ | 119.58 | 120.58 | 119.78 | 119.80 | 130.03 | 127.35 | N/A | 123.61 | 128.69 | 111.34 |
| 5′ | 119.82 | 120.58 | 119.78 | 119.80 | 125.81 | 126.99 | N/A | 127.30 | 127.29 | 120.05 |
| 6′ | 126.74 | 127.45 | 127.56 | 127.31 | 132.43 | 127.35 | 131.18 | 128.62 | 123.72 | 122.19 |
| 7′ | 126.56 | 126.84 | 126.99 | 127.29 | — | — | — | — | — | 120.78 |
| 8′ | 124.98 | 120.58 | 127.69 | 124.49 | — | — | — | — | — | — |
| 9′ | 37.33 | 56.88 | 56.88 | 55.89 | — | — | — | — | — | — |
| 4′a | 140.85 | 140.80 | 142.40 | 141.79 | — | — | — | — | — | — |
| 4′b | 141.49 | 141.13 | 142.40 | 141.81 | — | — | — | — | — | — |
| 8′a | 143.42 | 144.51 | 144.94 | 145.51 | — | — | — | — | — | — |
| 9′a | 143.42 | 147.29 | 144.94 | 146.17 | — | — | — | — | — | — |
| 1″ | — | — | — | — | 144.44 | 140.69 | 141.38 | 141.31 | 141.70 | — |
| 2″ | — | — | — | — | 128.00 | 128.03 | 129.60 | 127.25 | 127.22 | — |
| 3″ | — | — | — | — | 129.13 | 129.10 | N/A | 128.62 | 128.72 | — |
| 4″ | — | — | — | — | 127.23 | 130.11 | N/A | 125.55 | 125.97 | — |
| 5″ | — | — | — | — | 129.13 | 129.10 | N/A | 128.62 | 128.72 | — |
| 6″ | — | — | — | — | 128.00 | 128.03 | 129.60 | 127.30 | 127.22 | — |
| 9 | — | — | — | — | — | — | 66.91 | — | — | — |
| 3′a | — | — | — | — | — | — | — | — | — | 124.48 |
| 7′a | — | — | — | — | — | — | — | — | — | 136.87 |

The H2 signals of the major and minor forms coalesced at 243 K. These changes were also accompanied by resonance broadening and a change in integrated intensities. Similar results were also observed for $H4_{ax}$. On the other hand, the chemical shift and resonance broadening effects are minimal for the *N*-methyl resonances. The relative intensities changed with temperature, and the resonance due to the minor form disappeared at 243 K for all the three resonances. NOESY and ROESY data (not shown) confirmed the resonance assignments of the major and minor $H4_{ax}$, alkene, and *N*-methyl proton signals (Fig. 6D–F).

The assignments of the upfield resonances to *axial*-*N*-methyl and the downfield resonance to *equatorial*-*N*-methyl protons were based on γ-shielding and β-deshielding effects, respectively (Fig. 6C), and are in good agreement with published results.[24] The observation of well-resolved resonances for the *N*-methyl protons of the major and minor forms and a slower rate of

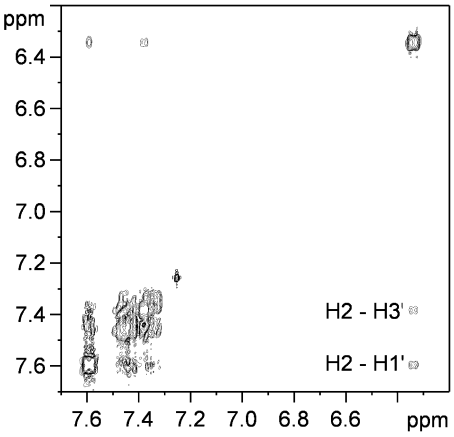


**Figure 4.** A NOESY cross-section of **8** showing the correlations of the H2 proton with aromatic protons of the proximal benzene ring.

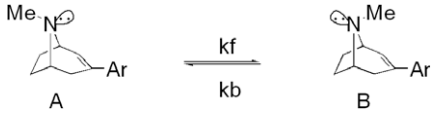


**Figure 5.** (A) *Equatorial* and (B) *axial* orientations of N-$CH_3$ in semi-rigid 3-aryl tropanes. $k_f$ and $k_b$ designate the forward and backward rate constants of the interconversion between *equatorial* and *axial* conformers.

interconversion in the NMR and dipolar relaxation time scales render the measurement of thermodynamic parameters by inversion magnetization transfer method feasible. The thermodynamic parameters for the interconversion between *axial* and *equatorial* conformers are shown in Table 3. The activation energy barriers vary significantly with the nature of the aryl groups. The analogs with bulky fluorenyl groups revealed large activation energies (29.5–36.7 kcal/mol). On the other hand, the activation energies of the flexible biaryl and naphthyl groups fell in the range of 15.9–18.3 kcal/mol. The significant differences in the energy barriers between the fluorenyl analogs and the biaryl derivatives demonstrate that even a small structural change in one part of the molecule can drastically alter the equilibrium dynamics in another part of the molecule; though the main structural difference between **1** and **8** is the absence of a second rotatable bond, the activation energy of the fluorenyl analog is twice (29.5 kcal/mol) that of the biaryl derivative (16.7 kcal/mol). The indole analog **9** displayed the lowest activation energy barrier (12.4 kcal/mol), which might be attributed to its size. The enthalpy of activation ($\Delta H^{\ddagger}$), entropy of activation ($\Delta S^{\ddagger}$), and free energy of activation ($\Delta G^{\ddagger,300K}$) were also estimated by using the Eyring equation and temperature-dependent rate constants. These thermodynamic parameters also reveal a trend similar to that of the activation energy barriers; the highest enthalpy and entropy changes were observed for **4** (36.4 kcal/mol, 112.6 cal/mol K), where as the lowest was observed for **9** (12.0 kcal/mol, −1.9 cal/mol K). In addition, the entropy of activation decreases as the steric bulk decreases and the rotational flexibility increases (95.3 cal/mol K for **4** to 9.72 cal/mol K for **9**). The difference in the thermodynamic parameters of the *forward* and *backward* reactions of a conformational equilibrium is also a measure of conformational preference. The *equatorial* form is favored in all the molecules except **9**. The extent of preference as determined by the relative magnitude of the difference falls in the order of **6** < **10** < **8** < **1** < **9** < **4** (Table 3).

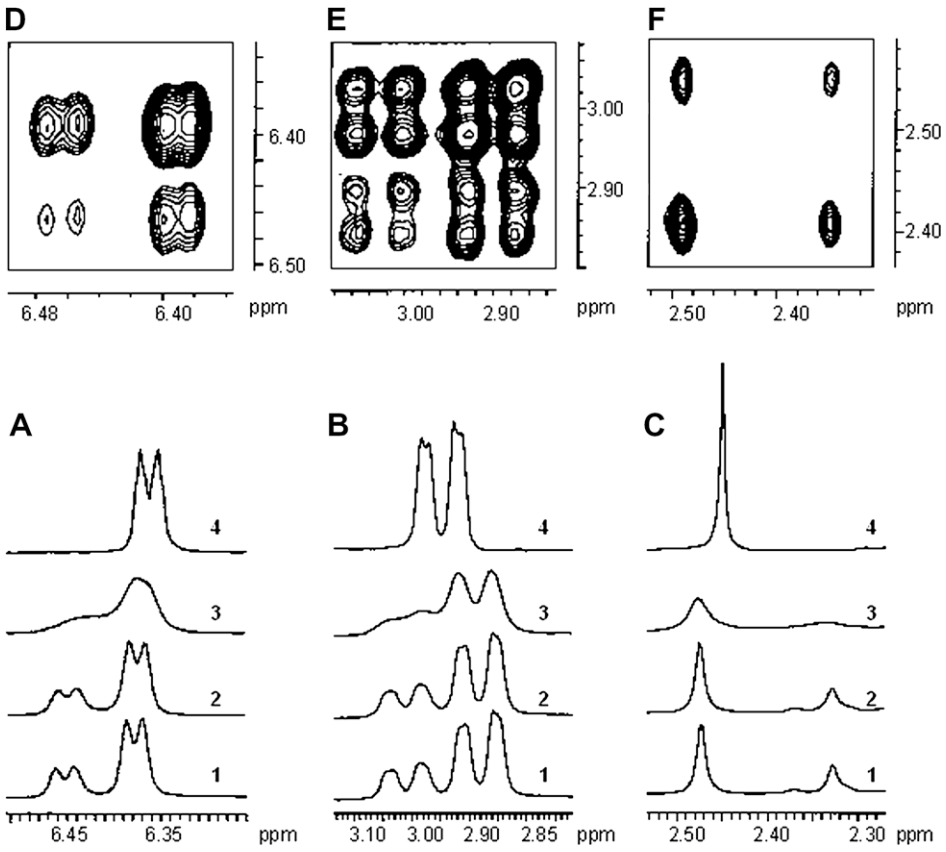


**Figure 6.** Temperature-dependent $^1$H spectra of (A) H2, (B) $H4_{ax}$, and (C) N–$CH_3$ for **8**. Traces: 1, 217 K; 2, 225 K; 3, 233 K; 4, 300 K. The J-splitting seen for H2 and $H4_{ax}$ is due to H1 and $H4_{eq}$, respectively. Corresponding exchange correlated peaks from NOESY experiment recorded at 217 K are shown in insets D–F.

**Table 3**
Thermodynamic parameters of nitrogen inversion for compounds **1**, **4**, **6**, **8**, **9**, and **10**

| Compound | Reaction | Parameters | | | | | | | | | |
|---|---|---|---|---|---|---|---|---|---|---|---|
| | | $E_a$[a] | $\Delta H^{\ddagger}_{NCH_3}$[a] | $\Delta S^{\ddagger}_{NCH_3}$[b] | $\Delta G^{\ddagger,300K}_{NCH_3}$[a] | $\Delta G^{\ddagger,243K}_{NCH_3}$[a] | $\Delta H^{oa,c}$ | $\Delta S^{ob,c}$ | $K$[d] | hDAT/hSERT | hNET/hSERT |
| **1** | ax → eq | 29.5 | 29.0 | 76.8 | 6.0 | 10.4 | 2.0 | 5.5 | 0.45 | 52.2 | 232 |
| | eq → ax | 31.5 | 31.0 | 87.7 | 4.7 | 9.7 | | | | | |
| **4** | ax → eq | 33.6 | 33.2 | 95.3 | 4.6 | 10.0 | 3.2 | 8.7 | 0.20 | 13.6 | 120 |
| | eq → ax | 36.7 | 36.4 | 112.6 | 2.6 | 9.0 | | | | | |
| **6** | ax → eq | 17.0 | 16.6 | 19.9 | 10.6 | 11.7 | 0.3 | 1.5 | 0.45 | 5.4 | 3.8 |
| | eq → ax | 17.4 | 16.9 | 23.0 | 10.0 | 11.3 | | | | | |
| **8** | ax → eq | 16.7 | 16.2 | 21.0 | 9.9 | 11.1 | 1.6 | 4.6 | 0.40 | 10.8 | 34 |
| | eq → ax | 18.3 | 17.8 | 30.1 | 8.8 | 10.5 | | | | | |
| **9** | ax → eq | 15.1 | 14.6 | 9.72 | 11.7 | 12.3 | −2.6 | −5.8 | 1.20 | 8.3 | 54 |
| | eq → ax | 12.4 | 12.0 | -1.9 | 12.6 | 12.4 | | | | | |
| **10** | ax → eq | 15.9 | 15.5 | 17.3 | 10.3 | 11.2 | 1.2 | 3.5 | 0.50 | 11.6[e] | 94.4[e] |
| | eq → ax | 17.1 | 16.6 | 24.2 | 9.4 | 10.8 | | | | | |

[a] Expressed in kcal/mol.
[b] Expressed in cal/mol deg.
[c] For N–$CH_3$ (standard deviation values are not shown).
[d] At 217 K.
[e] From Ref. 11.

Computational calculations and NMR studies of the interconversion between *equatorial* and *axial* conformers showed $\Delta G^{\circ}$ values between 1.1 and 1.5 kcal/mol for nitrogen inversion in cocaine and tropane analogs.[25,26] An *equatorial* conformer was found to be preferred in these studies. Earlier DNMR and NOE studies on the H2 resonance of **10** revealed different orientations of the naphthyl group for the major and minor form and proposed the conformational difference and the associated resonance doubling was the result of different orientations of the naphthyl group.[27] In the light of the new results that the major and minor forms originate from the *N*-methyl inversion, it is important to note that the process of nitrogen inversion is not 'silent' but introduces other structural changes such as favoring certain aryl orientations.

The free energy of activation ($\Delta G^{\ddagger,243K}$) at the coalescence temperature was also determined from the *N*-methyl (Table 3), H2 and $H4_{ax}$ resonances for **1**, **6**, and **8** by the method of Shanan-Atidi et al.[28] Similar magnitudes (~12.0 kcal/mol) of $\Delta H^{\dagger,243K}_{H_2}$, $\Delta H^{\dagger,243K}_{H_4}$, and $\Delta G^{\dagger,243K}_{NCH_3}$ and the increasing trend of equilibrium constants with temperature confirm that the origin of resonance doubling in H2 and $H4_{ax}$ is also due to nitrogen inversion (Supplementary Materials). The standard free enthalpy and standard free entropy changes (Table 3) computed using the van't Hoff equation also revealed a similar trend as the temperature independent $\Delta H^{\ddagger}$. Ratios of the two conformers at 217 K are very similar for **1**, **6**, **8**, and **10**, and the corresponding free energies of activation were found to be between 0.4 and 0.6 kcal/mol. *Axial* conformers make 40–50% of the total population in these molecules, a 5- to 10-fold increase over that of unsubstituted tropane. Exceptions are **4** ($\Delta G^{\circ}$ = 1.0 kcal/mol) and **9** ($\Delta G^{\circ}$ = 0.1 kcal/mol); in **4**, benzene rings on either side of the plane of the tropane ring interfere directly with the reorientation of the methyl group. A smaller pyrrole ring in **9** has the opposite effect, and *axial* conformer becomes the major form.

## 2.2. Three-dimensional solution structures of aryl tropane analogs

The three-dimensional solution structures of the aryl tropanes were derived from constrained molecular dynamic simulations (MDS). The number of NOE distance constraints varied between 10 and 20, and each molecule contained at least a few constraints determining the orientations of the aryl group with respect to the tropane system. The family of structures shown for individual compounds is within 2 kcal/mol of its lowest energy structure. The NOE constraints are compatible with *axial* as well as *equatorial* conformers for all the molecules except **6a**. The presence of $-CH_2Cl$ and the positive charge on the N8 shifted the equilibrium completely toward the *axial* form.

Compound **1** was found to exist in two families of substructures; the variation stems from the rotation around the $sp^2$–$sp^2$ bond (C2–C3–C2′–C1′-torsion angle) in combination with the N8 inversion. The average values of the torsional angles were found to be 129° and 55° with the methylene bridge group pointing above and below the plane of the tropane system, respectively. Since the low temperature NOESY experiment was able to detect the two conformations and allow for measurement of their interproton distances, it was possible to estimate the actual solution geometries **1B** and **1C** of compound **1** (Fig. 7). Rotation of the aryl substituent was accompanied by re-orientation of the *N*-methyl substituent from *equatorial*, relative to the piperidine ring, to *axial*. Whether this is a concerted process or an equilibrium exists between all possible forms is unknown.

The solution structure of compound **2** is influenced by the connection between two $sp^3$-hybridized carbons, C3 and C9′. The presence of the $sp^3$ carbon results in the staggered arrangement around

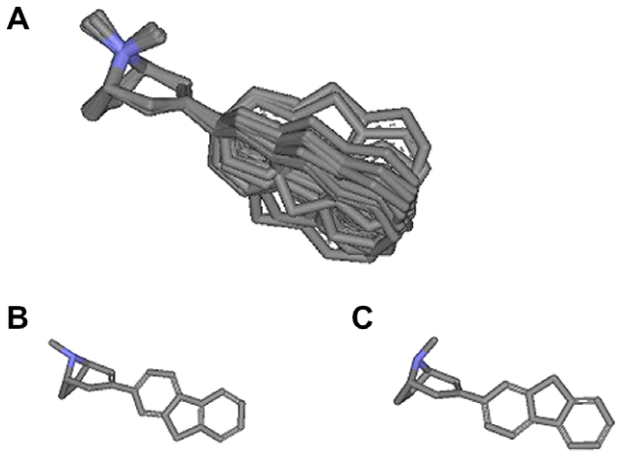


**Figure 7.** (A) Families of superimposed structures of **1**. Solution conformations of compound **1** detected at 217 K, (B) and (C). Color scheme: C, white; O, red; N, blue; H, not shown.

the $sp^3$–$sp^3$ single bond with the torsional angle being 171° so that the aromatic ring is tipped slightly on one side (H1′–$H2_{eq}$ distance is longer than H8′–$H4_{eq}$, 2.69 vs 2.44 Å). The aromatic rings of the fluorenyl substituent are oriented to the sides and below the plane of the tropane ring (Fig. 8A).

Similar situations are encountered with **3** (Fig. 8B), which lacks the bromine atom at C2′, thus having the plane of symmetry going through N8–C3–C9′, and C2–C3–C9′–C9a′ with a torsional angle of 162°. As a result, the NMR spectra are simplified and only one set of NOEs was detected marking the interaction of aromatic H1′ with $H2_{ax}$ and $H2_{eq}$. The distance estimates give 2.35 Å and 2.95 Å, respectively, similar to the values observed with **2**.

The introduction of the double bond in **4** changes the geometry of the whole molecule, as it can be seen from Figure 8C. The fluorenyl moiety is perpendicular to the tropane ring, but the presence of $sp^3$-hybridized single carbon bridge forces it out of orthogonality. The torsional angle defined by C2–C3–C9′–C9a′ linkage is 132°. The main features of NOESY data include the observation of NOE signals for H1′/H8′-H2 and H2-H9′ dipolar interactions and absence of NOE correlation signals between H1′/H8′ and $H4_{ax/eq}$. The aromatic protons H1′ and H8′ cannot be distinguished due to magnetic equivalence.

Changing the substituent to 2′-biphenyl in **5** and **6** (Fig. 9A and B) introduces the direct $sp^3$–$sp^2$ or $sp^2$–$sp^2$ linkages. In these cases, the distal benzene ring is located beneath the plane of the bicyclic ring, positioning the proximal ring in an almost orthogonal orientation (measured average torsional angle C2–C3–C2′–C1′ is −134°). The biphenyl rotation is limited around both single bonds. The presence of 3α-hydroxy group of **5** blocks the distal phenyl group, since it has to slide by it on the rotational path. When the hydroxyl is removed in the alkene analog **6**, rotational flexibility is introduced to some extent, and the resulting torsional angle decreases to 113°. Compound **6a** (Fig. 9C) also shows similar conformational restrictions. In addition, the *N*-methyl group is seen only in the *axial* orientation due to the bulky –$CH_2Cl$ occupying the *equatorial* orientation. The *axial* *N*-methyl group does not impose any hindrance for rotation of the biphenyl substituent around the tropane-aryl single bond. The NOE interactions between *N*-methyl and the biphenyl protons strongly support this conclusion.

Compounds **7** and **8** (Fig. 10A and B) assume two orientations of the biphenyl group either below or above the plane defined by the tropane ring. Two sets of NOE correlation peaks were observed at room temperature for the interactions between H2′ and $H2_{ax/eq}$ and H4′ and $H4_{ax/eq}$. As seen in **1**, the NOE derived geometries consist of two subfamilies due to the signal averaging of the NOE signals at room temperature. The C2–C3–C3′–C2′ torsional angles fall between 1° and −103°. Both alcohol **7** and its alkene counterpart **8** display significant rotational freedom at both rotatable bonds. A higher rate of rotation in **8** translates into averaging of distances for the interactions of H2′/H4′ and $H4_{ax/eq}$ (2.34 and 3.06 Å for **7** vs 2.57 and 2.84 Å for **8**). The two subfamilies in Figure 10 are present in 2:1 ratio based on low temperature NMR studies. The torsional angle between benzene rings was found to be in the range of −49 to −61°, defined with H2′–H2″ and H6′–H6″ NOE distance correlations.

The indole derivative, **9**, is the only ligand containing a heteroaromatic 3-aryl substituent. The smaller five-membered pyrrole ring provides additional rotational flexibility around the $sp^2$–$sp^2$ bond (Fig. 11). The torsional angle C2–C3–C3′–C2′ between the indole and the double bond moved away from orthogonality to ±128°, consequently. There is no evidence for rotation around the $sp^2$–$sp^2$ bond at room temperature (H4′–H4 and H2′–H2 NOE correlations), and the indole moiety is assumed to adopt the orientation represented in Figure 11. However resonance doubling

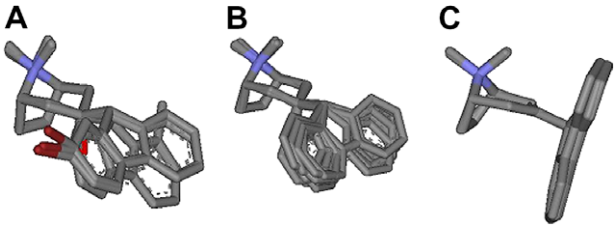


**Figure 8.** Families of superimposed structures for **2** (A), **3** (B), and 4 (C). Color scheme: C, white; O, red; N, blue; Br, magenta; H, not shown.

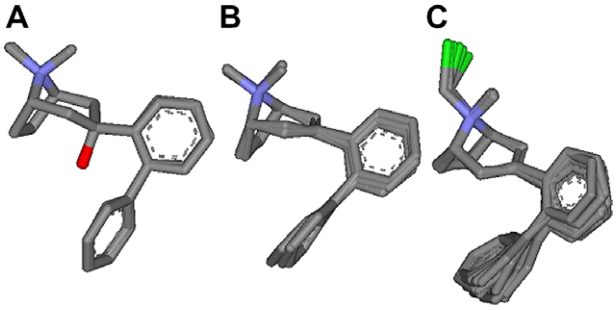


**Figure 9.** Families of superimposed structures for **5** (A), **6** (B), and **6a** (C). Color scheme: C, white; O, red; N, blue; Cl, green; H, not shown.

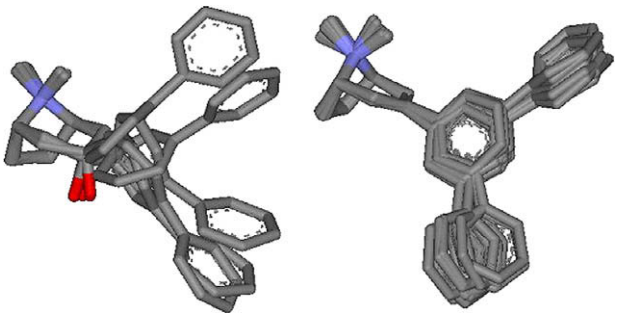

**Figure 10.** Families of superimposed structures for **7** (A) and **8** (B). Color scheme: C, white; O, red; N, blue; H, not shown.

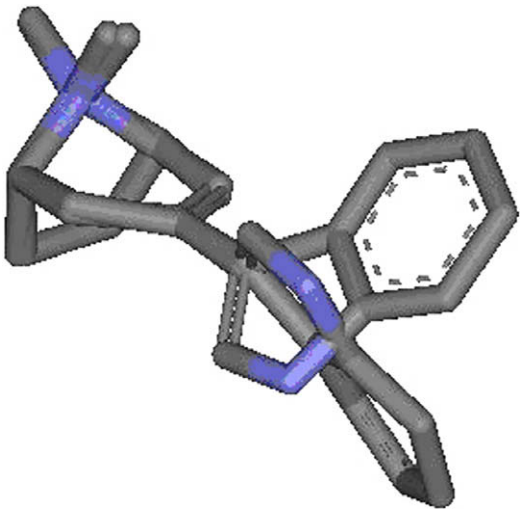

**Figure 11.** Family of superimposed structures for compound **9**. Color scheme: C, white; O, red; N, blue; H, not shown.

occurred at temperatures below 243 K, indicating *N*-methyl inversion.

Ligands containing an alkene bond in the tropane systems, **1**, **4**, **6**, **8**, and **9**, can be viewed as α,β-substituted styrenes fused with a tropane ring. In these molecules, the positions of atoms in C1–C2–C3 fragment are fixed, and the C3 position serves as a point of attachment for the aryl or heteroaryl group. This results in two possible orientations relative to the double bond (above and below the plane of the double bond). The aryl substituents are oriented in a manner that conjugation between the aryl and the double bond is diminished if not completely absent, which is further modified by the substitution on the proximal benzene ring. This, in turn, provides orthogonal or close-to-orthogonal orientation necessary for fitting tightly in the aryl-binding pocket of the monoamine transporter proteins. However, the aryl group rotation and the possibility of two orientations were absent (NOEs between H2 and H9′ for **4** and between H2–H2′ for **6** were only observed) for the fluorenyl and biphenyl derivatives **4** and **6**. The energy barriers for rotation may be too high.

The three commonly used computational modeling approaches to produce 3D conformations, systematic search (SyS), molecular dynamic simulation, and simulated annealing (SA) were applied initially as independent methods to derive plausible three-dimensional structures compatible with the NOE as well as DNMR data. In the course of the computational studies, it became evident that none of these approaches provided satisfactory results when applied individually. SyS possesses, for example, the capability of simultaneously rotating all rotatable bonds in a molecule. However, due to its inability to optimize the bond lengths and dihedral angles, SyS, in many cases, could not render conformations matching the NOE constraints. It is well known that MDS has the tendency of retaining a conformation at its local minima during the simulation process. Our modeling studies confirmed this notion—MDS only changed the geometry of the starting conformation to a limited extent even if the simulation temperature was raised to 700 K. Moreover, the inversion of the *N*-methyl group, indicated in the NMR conformational studies, was never found in any of the molecules during the MDS studies. On the other hand, it was found that SA was capable of providing multiple low energy conformations different from the starting conformation. The *N*-methyl inversion was also reflected during the SA simulation. However, the interproton distances of the final conformations deviated significantly from the experimental NOE constraints. Due to unsatisfactory performance of each of these approaches, a combination of the methods was used to address the conformational modeling requirements of the study. The SyS–MDS procedure was designed to utilize the capability of both SyS and MDS, SyS being able to select multiple conformations with different rotational angles, especially for the bond between the substituent and the tropane ring, and MDS being able to 'fine-tune' the bond lengths and angles to fit the NOE constraints. This procedure resulted in structures in which the distances did not deviate more than 5% from the experimental NOE constraints. The *N*-methyl inversion is also clearly evident in the final family of structures.

## 3. Conclusions

The solution structures and equilibrium dynamics of nitrogen inversion were characterized for a series of semi-rigid monoamine transporter ligands using NMR spectroscopy and molecular modeling. The non-polar medium used in this study is more representative of the environment encountered in the binding pockets of monoamine transporters. All of the 2,3-unsaturated 3-aryltropanes except the indole analog displayed a preference for the equatorial orientation of the $NCH_3$ group. The aryl group was found to be generally flexible, as a result of rotation around the single bond connecting the tropane and the aryl moiety. 3-Aryl tropanes lacking a 2-substituent retained moderate to high binding affinity and selectivity for the hSERT,[23] and considering these findings, it is evident that the aryl-binding pocket of the hSERT is quite tolerant to the steric bulk above and below the tropane ring, in addition to the *para* position of the proximal benzene ring. Another contributing factor to the selectivity for the hSERT is an increase in the population of an axially oriented *N*-methyl group, which is expected to be the binding conformation. Though the *equatorial* conformation was preferentially formed for the majority of the aryl tropenes investigated here, the equilibrium constants are much higher than those of either 2,3-substituted tropanes or the parent tropane molecule.[12,19,22,25]

The 2′-fluorenyl analog (compound **1**) displayed the highest affinity and selectivity for the hSERT. The orthogonal orientation of the aryl group relative to the tropane system and the 2:1 conformational equilibrium due to nitrogen inversion contribute significantly to this activity. In comparison, the second most active compound, the indole analog, has a 5-fold reduced potency for the hSERT. Unlike the other aryl substituents, the indole moiety was found to adopt conformations closer to co-planarity while the *N*-methyl equilibrium was shifted toward the *axial* form.

An aryl pharmacophore at position 3 of the tropane ring remains a major determinant of activity and selectivity for DAT/SERT. Fine tuning is possible through positioning of the lone electron pair of nitrogen, and the biphenyl analogs **6** and **8** represent good examples of this effect. Aryl substituents also influence the position of the *N*-methyl equilibrium, which in turn modulates the overall biological activity. Further investigation is required to determine the exact cause of this effect, either due to the steric factors and/or indirectly to the electron density of the double bond.[29] It is also possible that *N*-methyl reorientation and the rotation of the aryl substituent may occur simultaneously without one effect causing the other, as suggested by the low temperature NOE data.

## 4. Experimental

### 4.1. Synthesis of 3-aryl-8-*N*-methyl-8-azabicyclo[3.2.1]octanes

3-Aryl-substituted 8-methyl-8-azabicyclo[3.2.1]octanes (3-aryltropanes) and their 2,3-unsaturated analogs were synthesized using organolithium chemistry as described in Krunic et al.[23]

### 4.2. NMR Spectroscopy

$^1H$ and $^{13}C$ resonance assignments of all the molecules were determined using standard procedures with $^1H$, $^{13}C$, $^{13}C$-DEPT (distorsionless enhancement by polarization transfer) $^1H$–$^1H$ COSY (correlation spectroscopy), $^1H$–$^{13}C$ HMQC (heteronuclear multiple quantum coherence), $^1H$–$^{13}C$ HMBC (heteronuclear multiple bond correlation) and NOESY (Nuclear Overhauser effect spectroscopy) data. The solvent for the NMR samples was $CDCl_3$ (99.6%D from Sigma–Aldrich), and the chemical shifts were referenced from tetramethylsilane (TMS) unless mentioned otherwise. The temperature-dependent $^1H$ spectra were recorded in the range of 215–300 K, and the rate constants of interconversion were measured in the range of 217–237 K.

All the NMR data were collected at 300 MHz with a Bruker Avance DPX-300 spectrometer, and the 2D experiments were performed in phase sensitive mode with 2048 data points in the $t_2$-dimension and 512 data points in $t_1$-dimension. Zero-filling to 1024 points in $t_1$-dimension was employed prior to the second Fourier transformation. Sine window function was used in both the dimensions.

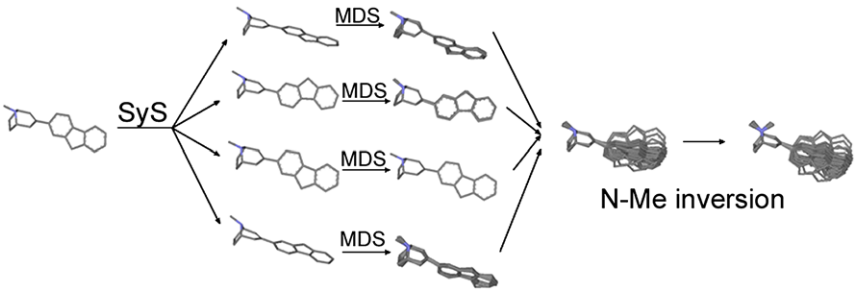


**Figure 12.** The general procedure for the NMR-based solution structure determination using the combination of systematic search and molecular dynamic simulations.

#### 4.2.1. Interproton distances

The interproton distance estimates for structure calculations were obtained through a series of 2D NOE experiments with variable mixing times ranging from 0.4 to 1.6 s. The NOE analysis was performed in the linear NOE build-up regime such that the two-spin approximation is valid. The interproton distances of various proton pairs were estimated by the following equation:

$$\sigma_{AB}/\sigma_{ref} = r_{ref}^6/r_{AB}^6$$

$\sigma_{AB}$ and $\sigma_{ref}$ denote the cross-relaxation constants of the dipolar vector connecting protons A and B and the dipolar vector connecting the reference protons. $r_{AB}$ and $r_{ref}$ denote the interproton distances between A and B, and between the reference proton pair, respectively. The cross-relaxation constants were estimated by fitting the initial NOE build-up to a straight line, as shown by the following equation:

$$NOE_{AB}(\tau_m) = -\sigma_{AB} * \tau_m + \text{Constant}$$

where $NOE_{AB}(\tau_m)$ denote the nuclear Overhauser effect at a mixing time of $\tau_m$ in seconds corresponding to the dipolar interaction between A and B, respectively. Methylene and *ortho* aromatic protons, for example, $H6_{exo}$–$H6_{endo}$, $H4_{exo}$–$H4_{endo}$, $H7_{exo}$–$H7_{endo}$, H3′–H4′, H4′–H5′, and H5′–H6′, were commonly used as reference proton pairs for the structure calculations. The nature and the number of reference distances used in the quantitative NOE calculations for a given molecule were limited by the resonance overlap. The reference distances of 1.78 Å and 2.45 Å were used, respectively, for methylene and aromatic *ortho*-proton pairs.

#### 4.2.2. Rate constants of *N*-methyl inversion

Rate constants of *N*-methyl inversion between the *axial* and *equatorial* conformers were measured by the inversion magnetization transfer method. In this method, the resonance of the major conformer is selectively inverted with the intensity of the minor conformer, followed with change in mixing time ($\tau_m$).[30] Mixing time, $\tau_m$, was varied between 0.00005 and 20.0 s and 13 $\tau_m$ values were used for each magnetization transfer run. Due to resonance overlap, intensities rather than integrated intensities were used in estimating the rate constants.

Magnetization transfer experiments were repeated 12 times at each temperature for **1** to determine the error associated with the estimated rate constants. The error in rate constants varied between 2% and 8% and resulted in similar deviation from the thermodynamic parameters determined with a single measurement.

### 4.3. Molecular modeling and structure calculations

All structure calculations were performed on Sybyl.[31] The initial 3D structures of the molecules were constructed in Sketcher, and Gasteiger-Hückel charges were calculated. First, the structures were minimized with both Steepest Descent and Conjugated Gradient methods using Tripos force field. Second, systematic search was performed on the minimized structures to identify the most plausible conformations with appropriate torsional angles. The torsional angle of the bond connecting the tropane ring and the aryl substituent was incremented in 1° steps where as that of other non-essential rotatable bonds was incremented in 30° steps. In the next round, the representatives of each set of conformations identified from SyS were subjected to constrained MDS optimization at 300 K in vacuum. The NOE constraints from the NMR study were applied to restrict the distances between corresponding hydrogen atom pairs. The conformations within 2 kcal/mol from the lowest energy conformer were initially selected as the candidate conformations, and finally, the conformations with <5% distance discrepancy from the NOE determined distances were identified as the final NMR structures. The molecular modeling procedure used to generate the solution structures is presented in Figure 12.

In order to evaluate and compare the performance of computational methods, simulated annealing (SA) was also applied in addition to systematic search and molecular dynamic simulations. Tripos force field and default parameters were used for SA. However, in the SA analysis, the annealing was conducted or ten cycles with the highest temperature of 700 K for 1000 fs and the lowest of 200 K for 1000 fs.

## Acknowledgment

A.K. wishes to express particular gratitude to Dr. Aleksandra Nenadic from the University of Manchester in the United Kingdom for writing a Java script for kinetic data analysis.

## Supplementary data

Supplementary data associated with this article can be found, in the online version, at doi:10.1016/j.bmc.2008.11.038.

## References and notes

1. Reith, M. E. A.; Sershen, H.; Allen, D. L.; Lajtha, A. *Mol. Pharmacol.* **1983**, *23*, 600.
2. Javitch, J. A.; Blaustein, R. O.; Snyder, S. H. *Mol. Pharmacol.* **1984**, *26*, 35.
3. Singer, H. S.; Hahn, I. H.; Moran, T. H. *Ann. Neurol.* **1991**, *30*, 558.
4. Ritz, M. C.; Boja, J. W.; Grigoriadis, D.; Zaczek, R.; Carroll, F. I.; Lewin, A. H.; Kuhar, M. J. *J. Neurochem.* **1990**, *55*, 1556.
5. Singh, S. *Chem. Rev.* **2000**, *100*, 925.
6. Carroll, F. I.; Gao, Y. G.; Rahman, M. A.; Abraham, P.; Parham, K.; Lewin, A. H.; Boja, J. W.; Kuhar, M. J. *J. Med. Chem.* **1991**, *34*, 2719.
7. Carroll, F. I.; Mascarella, S. W.; Kuzemko, M. A.; Gao, Y.; Abraham, P.; Lewin, A. H.; Boja, J. W.; Kuhar, M. J. *J. Med. Chem.* **1994**, *37*, 2865.
8. Carroll, F. I.; Gao, Y.; Abraham, P.; Lewin, A. H.; Lew, R.; Patel, A.; Boja, J. W.; Kuhar, M. J. *J. Med. Chem.* **1992**, *35*, 1813.
9. Carroll, F. I.; Kuzemko, M. A.; Gao, Y.; Abraham, P.; Lewin, A. H.; Boja, J. W.; Kuhar, M. J. *Med. Chem. Res.* **1992**, *1*, 382.
10. Blough, B. E.; Keverline, K. I.; Nie, Z.; Navarro, N.; Kuhar, M. J.; Carroll, F. Y. *J. Med. Chem.* **2002**, *45*, 4029.
11. Appell, M. D.; Dunn, W. J., III; Reith, M. E. A.; Miller, L.; Flippen-Anderson, J. L. *Bioorg. Med. Chem.* **2002**, *10*, 1197.
12. Belstotskii, A. M.; Goren, Z.; Gottlieb, H. E. *J. Nat. Prod.* **2004**, *67*, 1842.

13. Smith, M. P.; Johnson, K. M.; Zhang, M.; Flippen-Anderson, J. L.; Kozikowski, A. P. *J. Am. Chem. Soc.* **1998**, *120*, 9072.
14. Gabe, E. J.; Barnes, W. H. *Acta Crystallogr.* **1963**, *16*, 796.
15. Shen, M.; Ruble, J. R.; Hite, G. *Acta Crystallogr.* **1975**, *B31*, 2706.
16. Kelly, J. A.; Knox, J. R.; Lazer, E. S.; Nieforth, K. A. B.; Hite, G. *Acta Crystallogr.* **1977**, *B33*, 3542.
17. Hrynchuk, R. J.; Barton, R. J.; Robertson, B. E. *Can. J. Chem.* **1983**, *61*, 481.
18. Froimowitz, M. J. *J. Comp. Chem.* **1993**, *14*, 934.
19. Glasser, R.; Peng, Q.-J.; Perlin, A. S. *J. Org. Chem.* **1988**, *53*, 2172.
20. Bishop, R. J.; Fodor, G.; Katritzky, A. R.; Sotti, F. L.; Sutton, E.; Swinbourne, F. J. *J. Chem. Soc. C* **1966**, *1*, 74.
21. Casy, A. F.; Coates, J. E. *Org. Mag. Reson.* **1974**, *6*, 441.
22. Schneider, H.-J.; Sturm, L. *Angew. Chem.* **1976**, *88*, 574.
23. Krunic, A.; Mariappan, S. V. S.; Reith, M. E. A.; Dunn, W. J., III *Bioorg. Med. Chem. Lett.* **2005**, *15*, 5488.
24. Eliel, E. E.; Pietrusiewicz, K. M.. In *Topics in Carbon-13 NMR Spectroscopy*; Levy, G. C., Ed.; Wiley: New York, 1979; Vol. 3, p 172.
25. Belostotskii, A. M.; Shkokhen, M.; Gottlieb, H. E.; Hassmer, A. *Chem. Eur. J.* **2001**, *7*, 4715.
26. Zhu, N.; Harrison, A.; Trudell, M. L.; Klein-Stevens, C. L. *Struct. Chem.* **1999**, *10*, 91.
27. Appell, M. D.; Krunic, A.; Choi, T. J.; Mariappan, S. V. S.; Dunn, W. J., III; Reith, M. E. A. *QSAR* **2002**, *21*, 38.
28. Shanan-Atidi, H.; Bar-Eli, K. H. *J. Phys. Chem.* **1970**, *74*, 961.
29. Yoshikawa, K.; Bekki, K.; Karatsu, M.; Toyoda, K.; Kamio, T.; Morishima, I. *J. Am. Chem. Soc.* **1976**, *98*, 3272.
30. Mariappan, S. V. S.; Rabenstein, D. L. *J. Mag. Reson.* **1992**, *100*, 183.
31. SYBYL (Version 6.9), Tripos, Inc., 1699 South Hanley Road, St. Louis, MO 63144.